Journal of Computational Design and Engineering 5 (2018) 215–231

Contents lists available at ScienceDirect

Journal of Computational Design and Engineering

journal homepage: www.elsevier.com/locate/jcde

Optimum synthesis of oscillating slide actuators for mechatronic applications

P.A. Simionescu

Texas A&M University - Corpus Christi, 6300 Ocean Dr., Corpus Christi, TX 78412, United States

A R T I C L E I N F O

Article history:
Received 2 April 2017
Received in revised form 22 September 2017
Accepted 24 September 2017
Available online 25 September 2017

Keywords:
Slider-crank inversion
Limit positions
Transmission angle
Mechanical advantage
Uniform motion
Optimization

A B S T R A C T

The oscillating-slide inversion of the slider-crank mechanism, commonly symbolized RPRR, is widely used to convert the displacement of an input linear motor (either electric, hydraulic or pneumatic), into the swing motion of a rocker. This paper discusses the optimum kinematic synthesis of the centric RPRR mechanisms for prescribed limit positions, while simultaneously satisfying either (i) minimum deviation from 90° of its transmission angle, (ii) maximum mechanical advantage, or (iii) linear correlation between the input- and output-link motions. To assist practicing engineers, step-by-step design procedures, together with performance charts and parametric design charts are also provided in the paper.

1. Introduction

The centric *oscillating-slide* with translating input or RPRR in short (where the underscore indicates a powered joint), also known as *cylinder-incline*, *turning-block* or *swinging-block* linkage (Reifschneider, 2005; Yu, Huang, & Chieng, 2004) is one of the most widely used inversion of the slider-crank mechanism. It has numerous applications in robotics and industrial automation, aerospace, automotive, agricultural and earth moving machinery, etc. where it serves to convert the input motion of a linear actuator into partial rotation of an output-link rocker (Bagci, 1987; Hain, 1960, 1968; Söylemez, 2009; Zhang & Zhang, 2012) (Fig. 1).

The synthesis of the centric RPRR mechanism for prescribed limit positions of the output link, given the minimum and maximum lengths of the linear motor, can be relatively easily performed graphically (Bagci, 1987; Hartenberg & Denavit, 1964; Tao, 1964). There is no guarantee however that best motion transmitting characteristics are achieved, quantified by the *transmission angle* (Sandor & Erdman, 1984; Volmer, 1978) or by the *mechanical advantage* (Söylemez & Tönük, 1993; Yu et al., 2004). In addition, there are applications where a linear correlation between input and output is desired, such that the need for an additional encoder on the rocker shaft is eliminated (Karlsson & Gilmer, 2017).

This paper investigates through repeated optimizations and bivariate plots (Simionescu & Smith, 2000) the synthesis of centric RPRR oscillating-slide actuators for a prescribed rocker swing, given the fully retracted and fully extended lengths of the linear motor, while ensuring, throughout the motion range of the mechanism either of the following requirements: (i) minimum deviation from 90° of the transmission angle, (ii) maximum mechanical advantage, and (iii) a near-linear correlation between input and output motions.

Transmission angle (noted μ throughout the paper) should not depart more than ±45° from the ideal value of 90°. If a self-return of the output link is ensured by gravitational or elastic forces, transmission-angles ranging between 30° and 150° are still regarded as satisfactory (Hartenberg & Denavit, 1964; Sandor & Erdman, 1984; Söylemez, 2009).

In most applications, the gravitational and inertia forces acting upon the actuator of a centric RPRR mechanism are small relative to the load forces. Therefore, the linear motor will act as a two-force member i.e. the reaction forces between the piston and the cylinder (or equivalent) will be small, which is a major advantage over the PRRR slider-rocker mechanism actuators (Simionescu, 1999, 2016). However, if piggyback-hydraulic cylinder or side-bracketed electrical-actuators are employed (Fig. 2), these transverse forces can no longer be neglected. In addition, the designer should be concerned of the actuator not to buckle under load, particularly when slender linear actuators are utilized.

Peer review under responsibility of Society for Computational Design and Engineering.
E-mail address: pa.simionescu@tamucc.edu

https://doi.org/10.1016/j.jcde.2017.09.002
2288-4300/© 2017 Society for Computational Design and Engineering. Publishing Services by Elsevier.

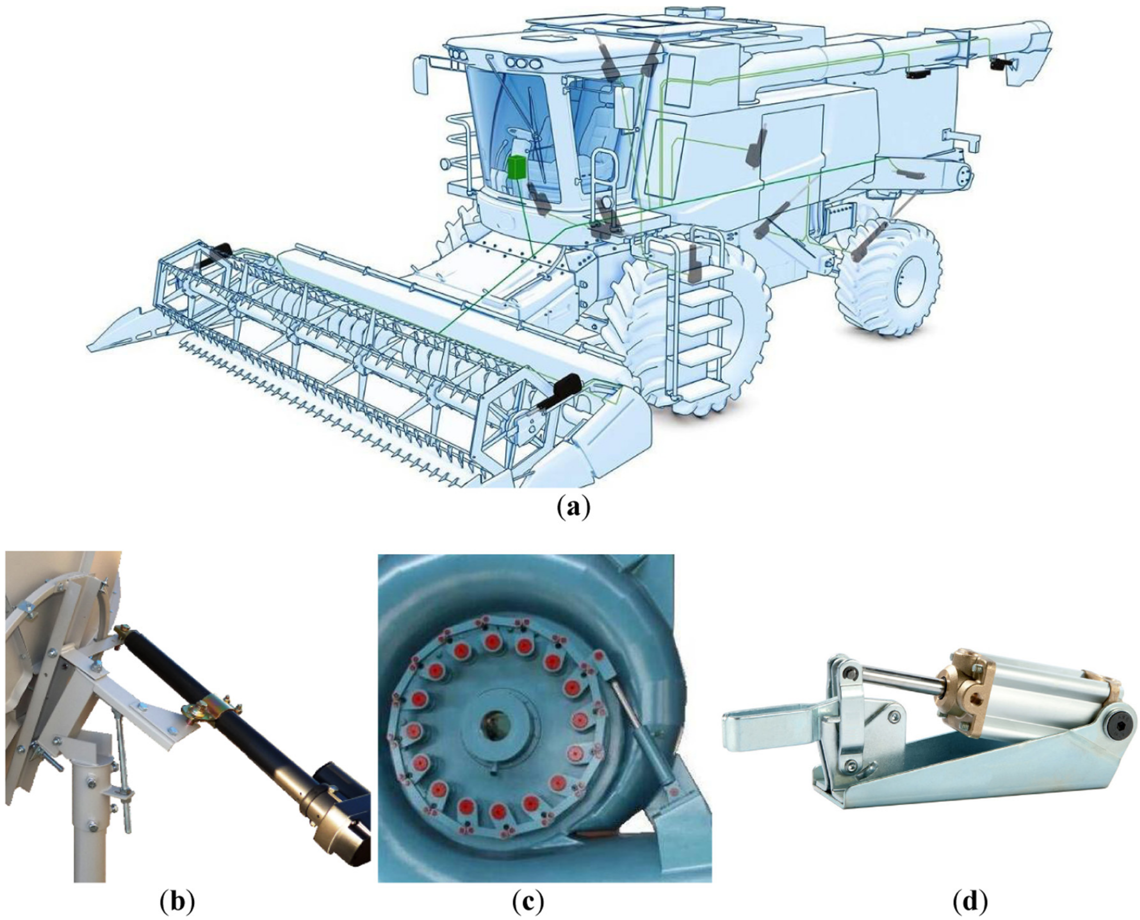

Fig. 1. Oscillating-slide actuator use in a harvesting combine (**a**), antenna or solar-panel tracker mechanism (**b**), wicket vane control of water turbines (**c**), and industrial automation (**d**) - photos courtesy of Thomson Industries, DH Solar, Zeco Turbines and Speedy Block.

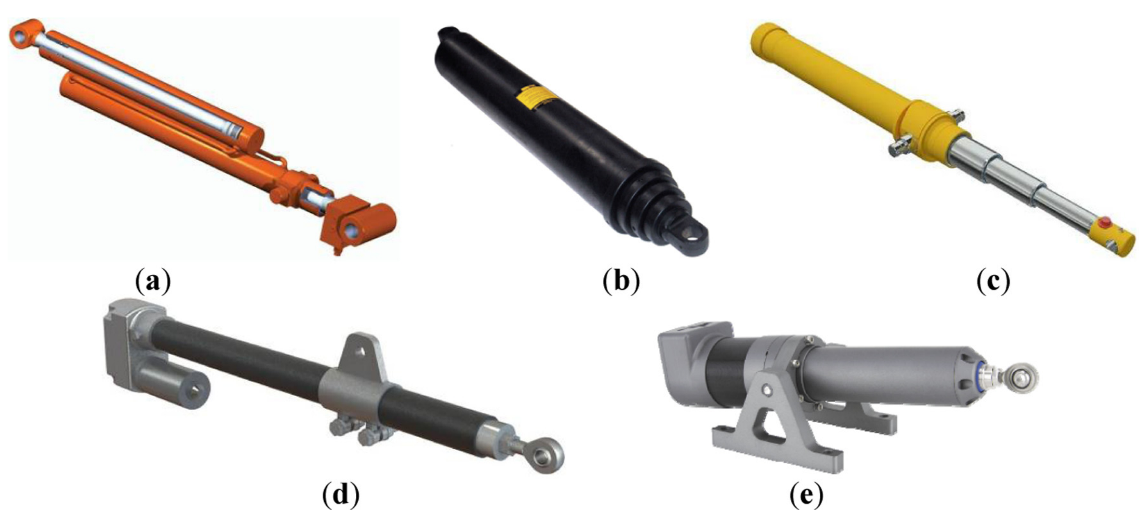

Fig. 2. Linear actuators: hydraulic (**a**) single-acting piggyback, (**b**) end-mounted telescopic, (**c**) trunnion-mounted telescopic, (**d**) side-bracketed electric and (**e**) trunnion-mounted electric (Parker Hannifin Corp, 2009; Eagle Hydraulic Components Inc, 2016; Texas Hydraulics, 2016; Ultra Motion, 2016; SKF, 2016).

2. Synthesis problem formulation

Fig. 3 depicts a centric RPRR oscillating-slide mechanism, loaded at the rocker with a constant moment M, which must be overcome by a position-dependent force P_j delivered by the linear motor. The angular stroke $\Delta\varphi$ of the output link is measured between its initial and final positions φ_s and φ_f defines as shown. The main design requirement upon this mechanism is to generate a prescribed rocker angle $\Delta\varphi = \varphi_f - \varphi_s$ when the linear-motor extends from its minimum length L_{min}, to its maximum length L_{max}, over a total displacement ΔL_{max}=$L_{max} - L_{min}$.

For the sake of generality, the kinematic calculations will be performed for the mechanism normalized with respect to the ground member, i.e. at all times $OA = 1.0$ (the final dimensions of

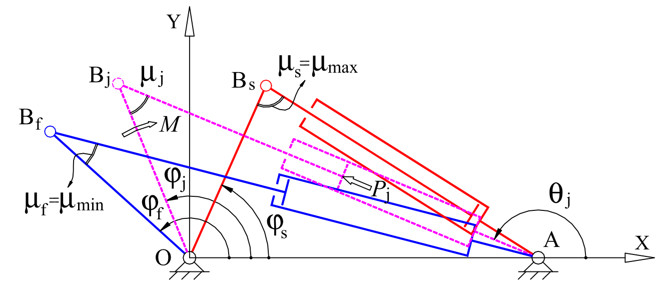

Fig. 3. Centric R<u>P</u>RR oscillating-slide mechanism loaded by a constant moment M applied at the rocker, shown in its initial position "s", in its final position "f", and in an arbitrary intermediate position "j".

the mechanism will be easily obtained post synthesis through proper scaling). Consequently, the capabilities of the actuator will be specified by its normalized minimum length AB_s, and by the extension coefficient K defined as:

$$K = \frac{AB_f}{AB_s} = \frac{L_{max}}{L_{min}} = 1 + \frac{S_{max}}{L_{min}} \tag{1}$$

Based on the data available in references (Parker Hannifin Corp, 2009; Eagle Hydraulic Components Inc., 2016; Texas Hydraulics, 2016; Ultra Motion, 2016; SKF, 2016), coefficient K of the linear motor was found to range between 1.25 and 1.8 for simple hydraulic or pneumatic cylinders, between 2.5 and 3 for piggyback cylinders, and between 3 and 4.7 for telescopic cylinders. Some telescopic cylinders with more than five stages, or of the trunnion-mounted type can extend over five times their fully retracted length (Ergo-Help Pneumatic, 2016), a case however not covered in this paper.

Given the initial rocker angle φ_s and extension coefficient K, the unknown normalized length OB and AB_s can be determined beginning with equations of constraint (2.a) and (2.b), written for the deformable triangular loop A–B–C (see Fig. 3):

$$AB_s^2 = (x_{Bs} - x_A)^2 + (y_{Bs} - y_A)^2 \tag{2.a}$$

$$AB_f^2 = (x_{Bf} - x_A)^2 + (y_{Bf} - y_A)^2 \tag{2.b}$$

where the x and y coordinates of joint B are:

$$x_{Bs} = OB \cdot \cos(\varphi_s) \qquad y_{Bs} = OB \cdot \sin(\varphi_s) \tag{3.a}$$

$$x_{Bf} = OB \cdot \cos(\varphi_f) \qquad y_{Bf} = OB \cdot \sin(\varphi_f) \tag{3.b}$$

For $x_A = 1$, $y_A = 0$ and $AB_f = K \cdot AB_s$ Eqs. (2) become:

$$AB_s^2 = OB^2 - 2 \cdot OB \cdot \cos(\varphi_s) + 1 \tag{4.a}$$

$$K^2 \cdot AB_s^2 = OB^2 - 2 \cdot OB \cdot \cos(\varphi_f) + 1 \tag{4.b}$$

After eliminating AB_s between Eqs. (4), a quadratic in the sought-for normalized rocker length OB is obtained i.e.

$$OB^2 - 2\frac{K^2 \cdot \cos(\varphi_s) - \cos(\varphi_f)}{K^2 - 1} OB + 1 = 0 \tag{5}$$

with solutions

$$OB = \frac{K^2 \cdot \cos(\varphi_s) - \cos(\varphi_f)}{K^2 - 1} \pm \sqrt{\left(\frac{K^2 \cdot \cos(\varphi_s) - \cos(\varphi_f)}{K^2 - 1}\right)^2 - 1} \tag{6}$$

The double sign "±" in Eq. (6) indicates that, for a given initial rocker angle φ_s, two mechanism solutions exist - a result also reported in Reifschneider (2005) and Simionescu (1999). The solution obtained for a minus sign in front of the square root in Eq. (6) will be called *short-rocker oscillating-slide mechanism*, while the one with a plus in front of the square root will be called *long-rocker oscillating-slide mechanism* (as seen in dump-truck beds actuated using telescopic cylinders).

Once the normalized rocker length OB has been found, the corresponding length AB_s of the fully retracted linear actuator (also normalized) can be calculated using Eq. (4.a).

Since rocker OB can theoretically assume any initial angle between 0° and 180°, φ_s can be tuned until additional design requirements are satisfied. One such requirement is for the transmission angle μ to exhibit minimum deviation from 90° over the entire working range of the mechanism. Given the displacement of the actuator AB_j, angle μ_j can be calculated using the equation:

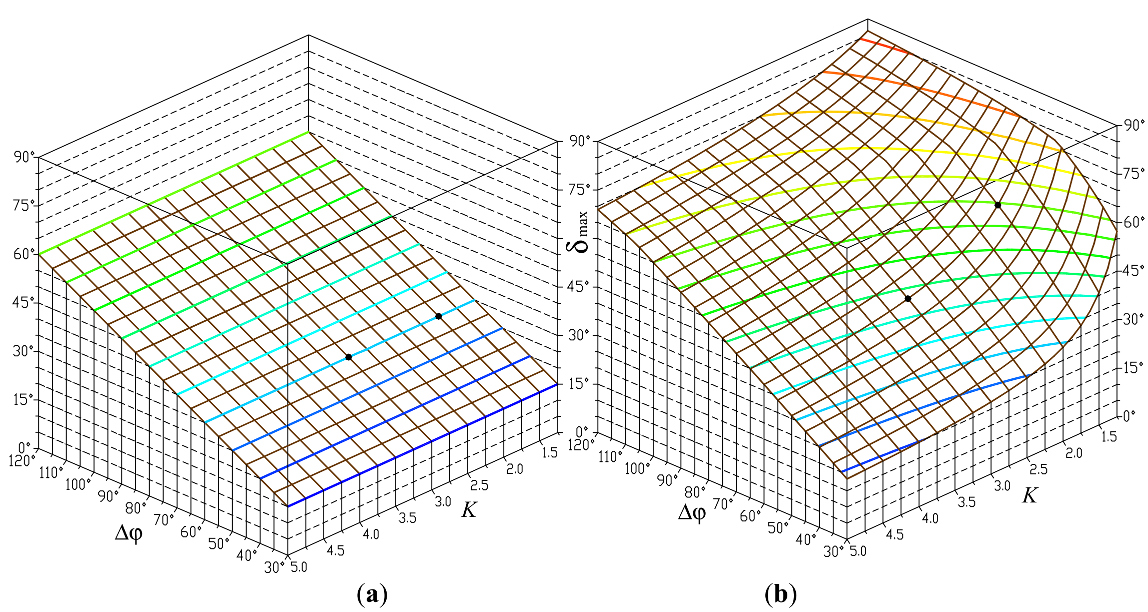

Fig. 4. Best transmission angle the R<u>P</u>RR mechanism is capable of. Plot (**a**) corresponds to short rocker mechanisms and plot (**b**) corresponds to long rocker mechanisms.

$$\cos\mu_j = \frac{OB^2 + AB_j^2 - 1}{2 \cdot OB \cdot AB_j} \tag{7}$$

In all practical RPRR oscillating-slide mechanisms, angles φ and μ will vary monotonically with the displacement of the slider. Therefore cos μ in Eq. (7) will also vary monotonically with the linear motor extension, and as a consequence, the maximum departure from 90° of angle μ will occur at the limit positions φ_s and φ_f. This property has been utilized in defining the following deviation function:

$$\delta^*_{max} = Max\{|\cos\mu_s|, |\cos\mu_f|\} \tag{8}$$

Another parameter of interest in the design of RPRR mechanisms is the *mechanical advantage*, equal to the *force-to-torque multiplication factor* (*FTMF*), and also equal to the inverse of the kinematic coefficient dφ/d*S* of the mechanism where *S* is the piston displacement (Bagci, 1987)

$$FTMF = \frac{M}{P} = \left(\frac{d\varphi}{dS}\right)^{-1} \tag{9}$$

For the centric RPRR oscillating-slide, an equivalent relationship can be derived from considerations of static equilibrium of the rocker that is:

$$FTMF = \frac{M}{P} = OB \cdot \sin(\mu) \tag{10}$$

Based on this latter equation, a second performance parameter of the mechanism has been defined i.e.

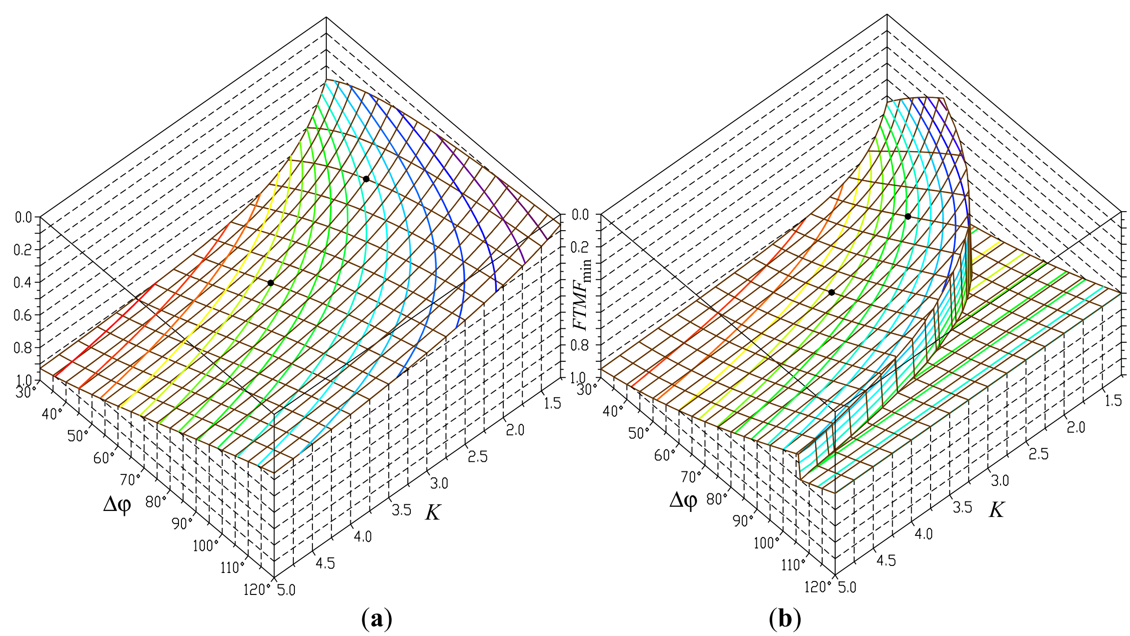

Fig. 5. Minimum *FTMF* of the RPRR mechanisms optimized for transmission angle. Plot (**a**) corresponds to short rocker mechanisms and plot (**b**) corresponds to long rocker mechanisms.

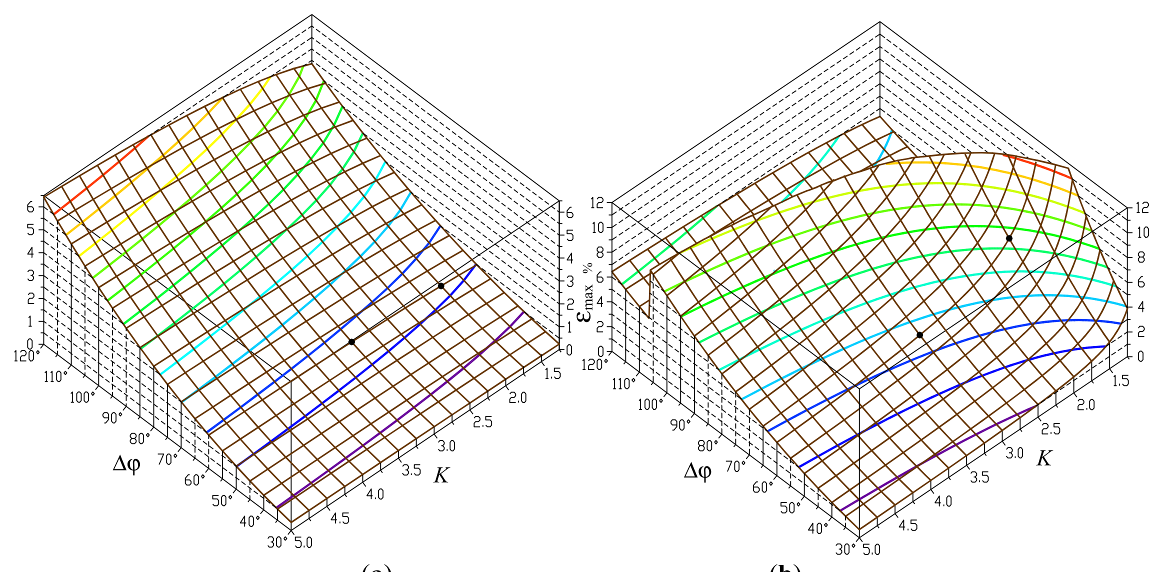

Fig. 6. Maximum linearity error of the RPRR mechanisms optimized for transmission angle. Plot (**a**) corresponds to short rocker mechanisms and plot (**b**) corresponds to long rocker mechanisms.

Table 1
Parameters of the RPRR mechanisms optimized for transmission angle with $\Delta\varphi = 60°$, $K = 1.75$ and $K = 3$.

	RPRR type	K	φ_s (°)	OA	OB	AB_s	δ_{max} (°)	ε_{max} (%)	$FTMF_{min}$
(a)	Short rocker	1.75	34.72	1.0	0.49320	0.65760	30.00	1.12	0.427
(b)	Short rocker	3.0	19.11	1.0	0.75593	0.37796	30.00	1.31	0.655
(c)	Long rocker	1.75	58.99	1.0	1.00	0.98466	59.49	6.48	0.508
(d)	Long rocker	3.0	26.37	1.0	1.00	0.45625	43.19	3.55	0.729

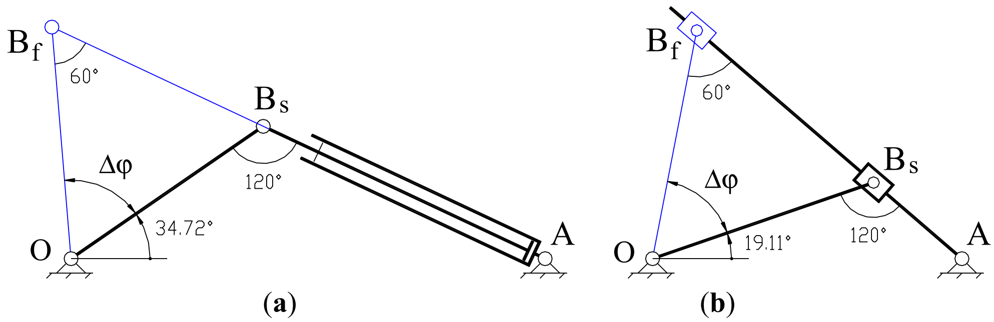

Fig. 7. Optimum mechanisms in Table 1, scaled such that their linear motor displacements ΔS_{max} are the same.

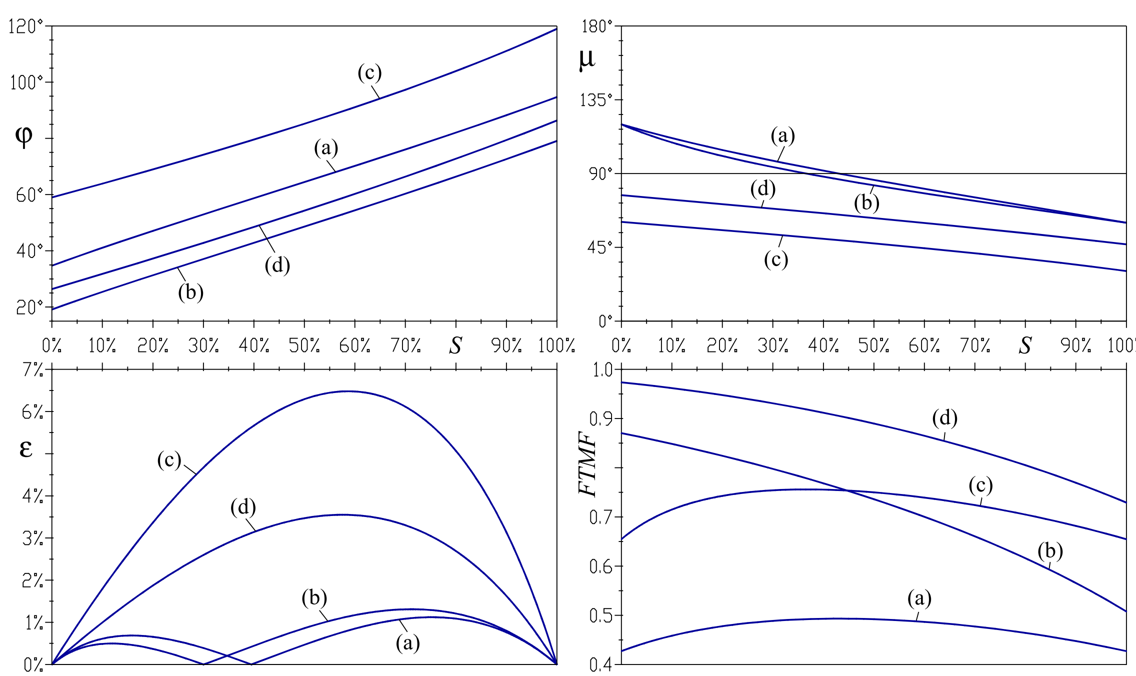

Fig. 8. Kinematic and performance diagrams of the mechanisms in Fig. 7, labeled the same as in Table 1 and Fig. 7.

$$FTMF_{\min} = \underset{j=1}{\overset{n}{Min}} |OB \cdot \sin(\mu_j)| \tag{11}$$

For a given torque-load M to be overcome with a minimum actuator force, $FTMF_{\min}$ should evidently be as big as possible.

In many control applications, it is of interest for the RP̲RR mechanism to ensure a close-to-linear I/O relationship $\varphi(AB)$ (Karlsson & Gilmer, 2017). Therefore a linearity-error function has been additionally defined:

$$\varepsilon = \left| \frac{AB_j - AB_s}{AB_f - AB_s} - \frac{\varphi_j - \varphi_s}{\Delta\varphi} \right| \tag{12}$$

where

$$\varphi_j = \cos^{-1}\left(\frac{OB^2 - AB_j^2 + 1}{2OB}\right) \tag{13}$$

What will actually be monitored during the design process is the *maximum-linearity error* function i.e.

$$\varepsilon_{\max} = \underset{j=1}{\overset{n}{Max}} |\varepsilon(AB_j)| \tag{14}$$

The number of discrete positions j in the above equations (11), (12) and (14) correspond to the length AB_j of the actuator taking n uniformly spaced values between $L_{\min}$ and $L_{\max}$.

3. Centric RP̲RR mechanism actuators optimized for transmission angle

A first design scenario considered is that of satisfying minimum deviation from 90° of the transmission angle. For this purpose, the maximum deviation angle in equation (8) has been minimized with respect to φ_s using a combination of the *Localmin* univariate

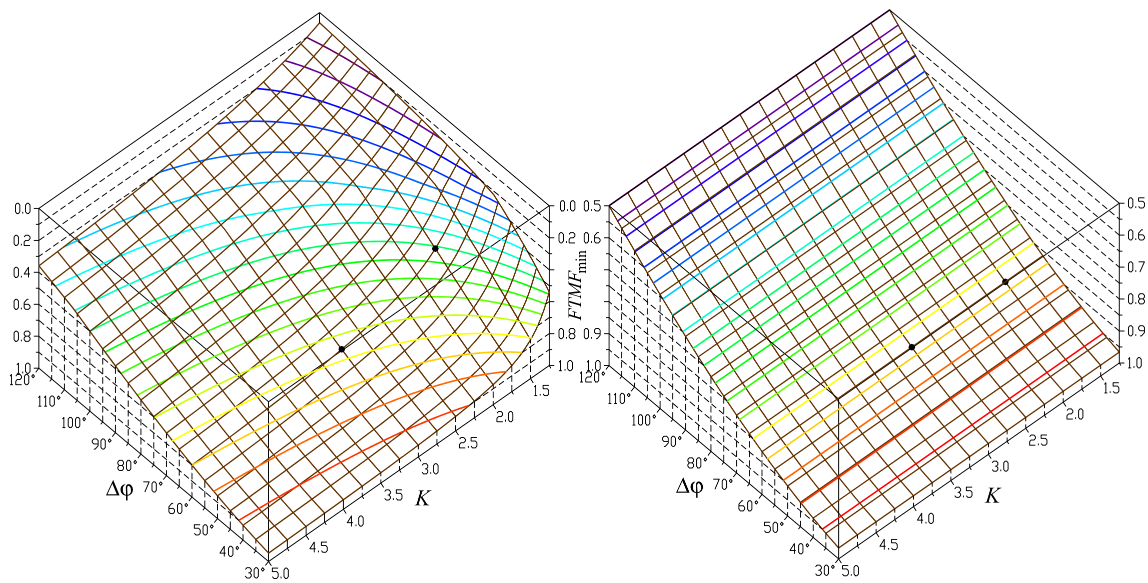

(a) (b)

Fig. 9. Best *FTMF* the centric RP̲RR mechanisms are capable of. Plot (**a**) corresponds to short rocker mechanisms and plot (**b**) corresponds to long rocker mechanisms.

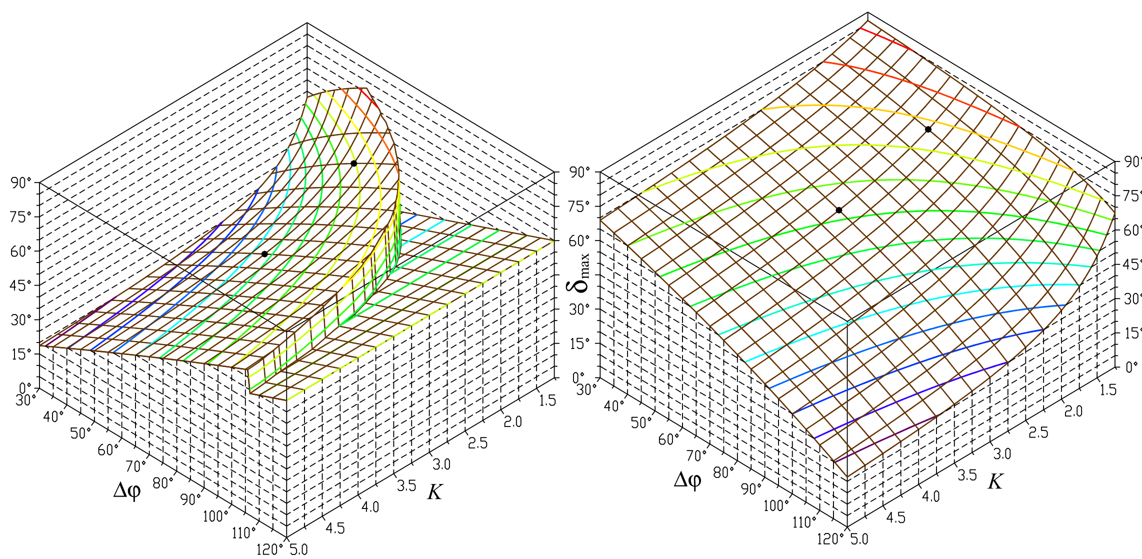

(a) (b)

Fig. 10. Maximum deviation of the transmission angle of the centric RP̲RR mechanisms optimized for mechanical advantage. Plot (**a**) corresponds to short rocker mechanisms and plot (**b**) corresponds to long rocker mechanisms.

minimization algorithm due to Brent, preceded by a grid search (Brent, 2013; Simionescu, 2014), for coefficient K and angle $\Delta\varphi$ ranging between 1.25 and 5, and between 30° and 120° respectively. The resulting data served to generate the 3D performance plots in Figs. 4 and 5, and the parametric plots in Appendix A. Note that the δ_{max} plot in Fig. 4 has been generated using values calculated with:

$$\delta_{max} = |arcos(\delta^*_{max}) - 90°| \tag{15}$$

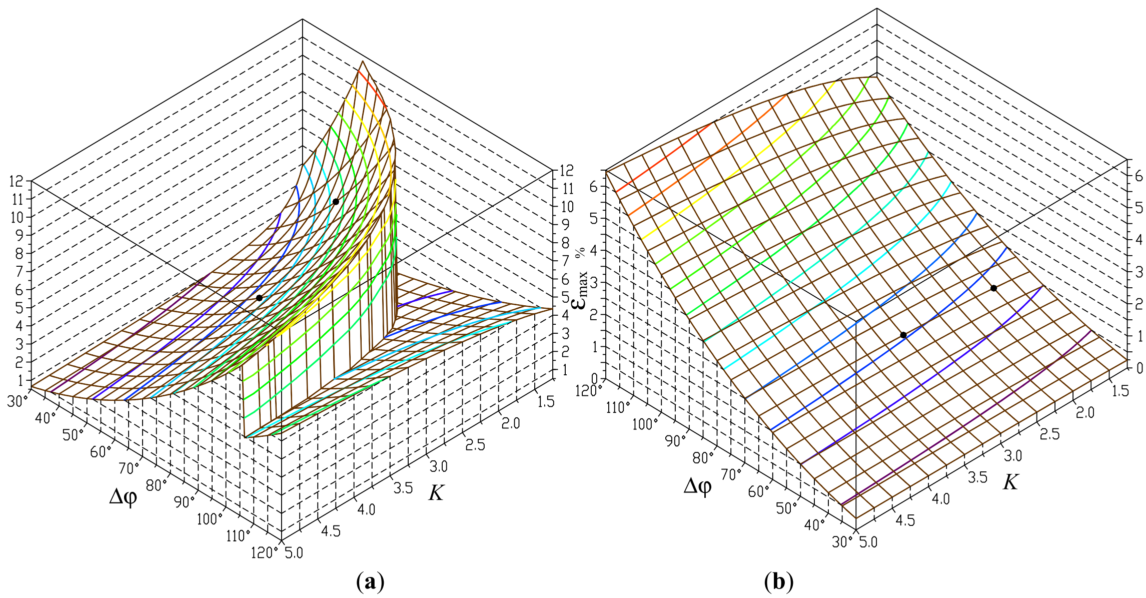

Fig. 11. Maximum linearity error of the centric R$\underline{P}$RR mechanisms optimized for mechanical advantage. Plot (**a**) corresponds to short rocker mechanisms and plot (**b**) corresponds to long rocker mechanisms.

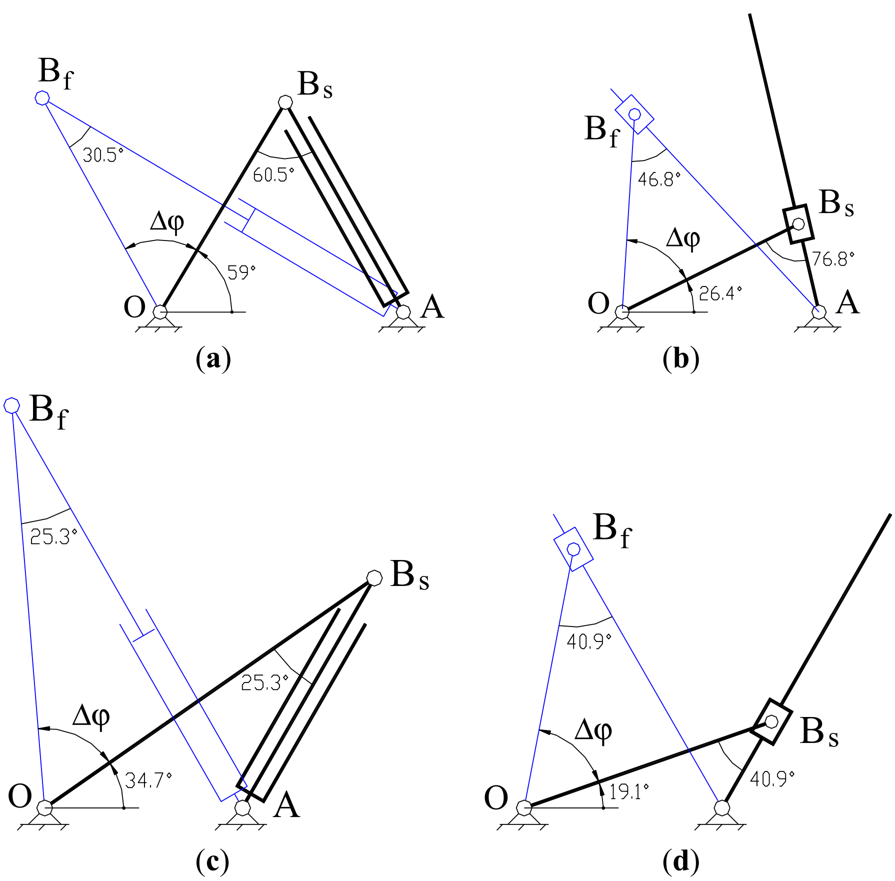

Fig. 12. Optimum mechanisms in Table 2, scaled such that their linear motor displacement ΔS_{max} is the same.

In order to avoid the occurrence of *order defects* (Sandor & Erdman, 1984), the objective functions defined throughout this paper have been penalized for the cases where vector loop O–A–B has different orientations in its initial and final positions. This has been done by evaluating the cross products $\mathbf{OB_s} \times \mathbf{B_sA}$ and $\mathbf{OB_f} \times \mathbf{B_fA}$ and verifying that they have the same sign. The minimization of $\delta^*_{max}(\varphi_s)$ for given angle $\Delta\varphi$ and extension coefficient K will return, in addition to the initial rocker angle φ_s for which the transmission angle has minimum deviation from 90°, the normalized lengths OB and AB_s.

Notice that the plots in Fig. 5b, 6b, A1b, A2b, and A3b exhibit discontinuities resembling *ha-ha walls* from landscape design. The areas inside these *walls* correspond to the following inequality:

$$\Delta\varphi - 0.4759K^5 + 8.3287K^4 - 57.79K^3 + 200.97K^2 - 361.12K + 179.91 \leqslant 0 \quad (16)$$

determined through numerical curve fitting.

Figs. 4–6 and A1–A3 provide an overview upon the performances and proportions of the centric RP̲RR mechanism optimized for transmission angle. To complement these plots, numerical examples of four oscillating slide mechanisms obtained by minimizing equation (8) will be discussed next. These are the centric (short and long rocker) RP̲RR mechanisms with $\Delta\varphi = 60°$, driven by linear actuators with $K = 1.75$ and $K = 3$ respectively. The normalized geometric parameters of these mechanisms are summarized in Table 1. They are also shown in Fig. 7 scaled such that their limit positions are attained for the same displacement ΔS_{max} of the actuator. Fig. 8 shows plots of the I/O function $\varphi(S)$, transmission angle $\mu(S)$, linearity error $\varepsilon(S)$ and *force-to-torque multiplication factor FTMF*(S) of the same mechanisms in Table 1. The parameters of the same mechanisms have been marked each with a dot on the 3D plots in Figs. 4–6 and in Appendix A. They are also available as animated GIF files generated as explained in Simionescu (2014) from the author's *ResearchGate* page, or upon request.

3.1. Comparison between the RP̲RR mechanisms with short and long rockers, optimized for transmission angle

The 3D plots and numerical examples presented earlier revealed several properties of the centric RP̲RR mechanisms with short and long rocker, optimized for transmission angle. These are as follow:

(1) For the same rocker angle $\Delta\varphi$, the short-rocker mechanisms have better transmission angles compared to the long-rocker mechanisms (Fig. 4).
(2) The transmission-angle performance of short-rocker mechanisms is not influenced by the extension coefficient K (Fig. 4a).
(3) The transmission angle μ of short-rocker mechanisms has symmetric deviation from 90°, equal to half the angle $\Delta\varphi$ of the rocker, and the difference between the minimum and maximum values of angle μ equals $\Delta\varphi$ - a property also

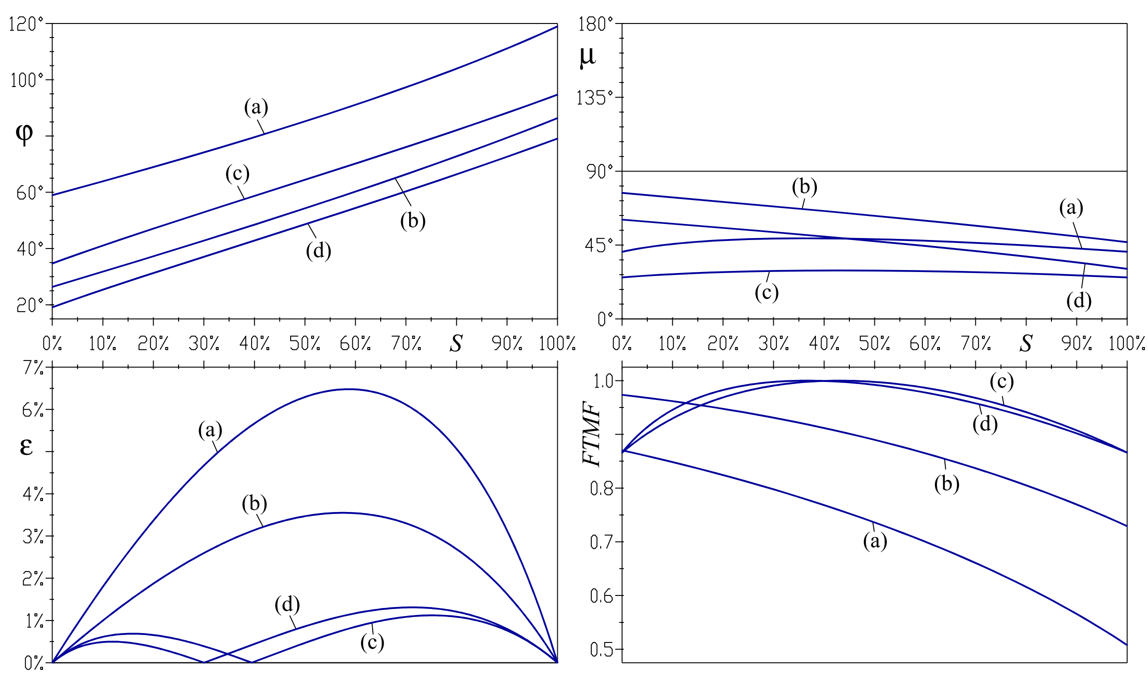

Fig. 13. Kinematic and performance diagrams of the mechanisms in Fig. 12, labeled the same as in Table 2 and in Fig. 12.

Table 2
Parameters of the RP̲RR mechanisms with $\Delta\varphi = 60°$, $K = 1.75$ and $K = 3$ that have been optimized for mechanical advantage.

	RP̲RR type	K	φ_s (°)	OA	OB	AB_s	δ_{max} (°)	ε_{max} (%)	$FTMF_{min}$
(a)	Short rocker	1.75	58.99	1.0	1.0	0.984655	59.49	6.48	0.508
(b)	Short rocker	3.0	26.37	1.0	1.0	0.456253	43.19	3.55	0.729
(c)	Long rocker	1.75	34.72	1.0	2.027588	1.333333	64.72	1.12	0.866
(d)	Long rocker	3.0	19.11	1.0	1.322876	0.5	49.11	1.31	0.866

reported in Söylemez (2009), Volmer (1978), and Simionescu (1999). This indicates that for Δφ in excess of 120°, the angle μ will vary more than ±60° from 90°, rendering the corresponding short-rocker RPRR mechanisms prone to jamming.

(4) The I/O function of short rocker mechanisms optimized for transmission angle are closer to being linear in comparison with that of the equivalent long-rocker mechanisms.
(5) Long-rocker RPRR mechanisms have their rocker length equal to their base length (Fig. A2b).
(6) Long rocker mechanisms should be used in association with large extension-coefficient actuators, and for the generation of rocker angles Δφ that are less than 100° (Fig. 4b).
(7) The transmission angle of a long-rocker mechanism with imposed Δφ angle can be improved by selecting a linear actuator with a larger extension coefficient *K* (Fig. 4b).

3.2. Design procedure of short-rocker RPRR mechanism with optimum transmission angle

An easy to apply graphical method of synthesizing a short-rocker RPRR mechanism with best transmission angle properties is as follows - see also Fig. 7a and b and references Simionescu (1999), Söylemez (2009), and Volmer (1978):

(1) Use equations

$$\mu_{\min} = 90^\circ - \Delta\varphi/2 \quad \text{and} \quad \mu_{\max} = 90^\circ + \Delta\varphi/2 \tag{17}$$

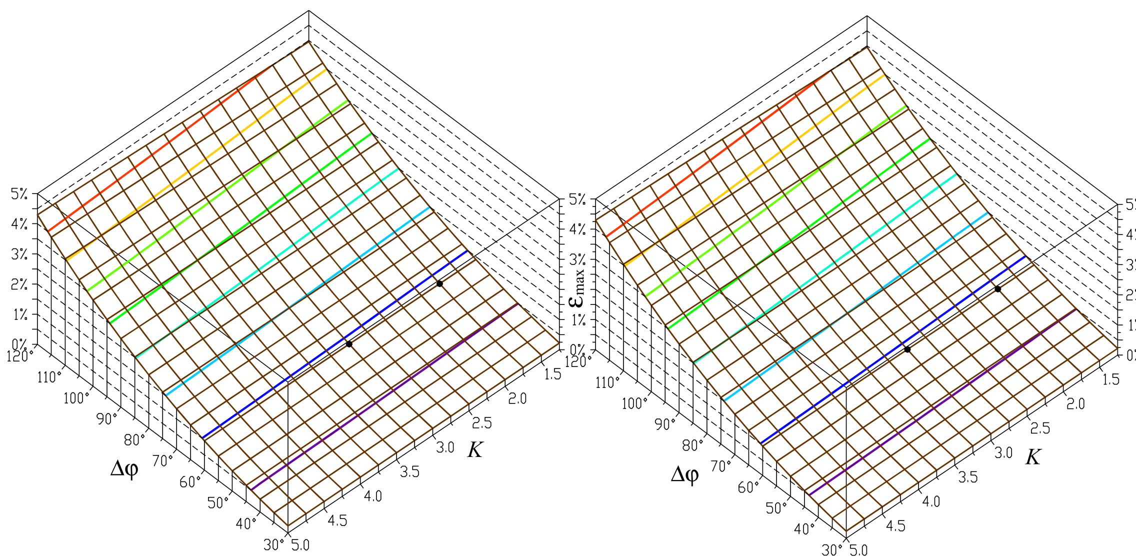

(**a**) (**b**)

Fig. 14. Minimum linearity errors the centric RPRR mechanisms are capable of. Plot (**a**) corresponds to short rocker mechanisms and plot (**b**) corresponds to long rocker mechanisms.

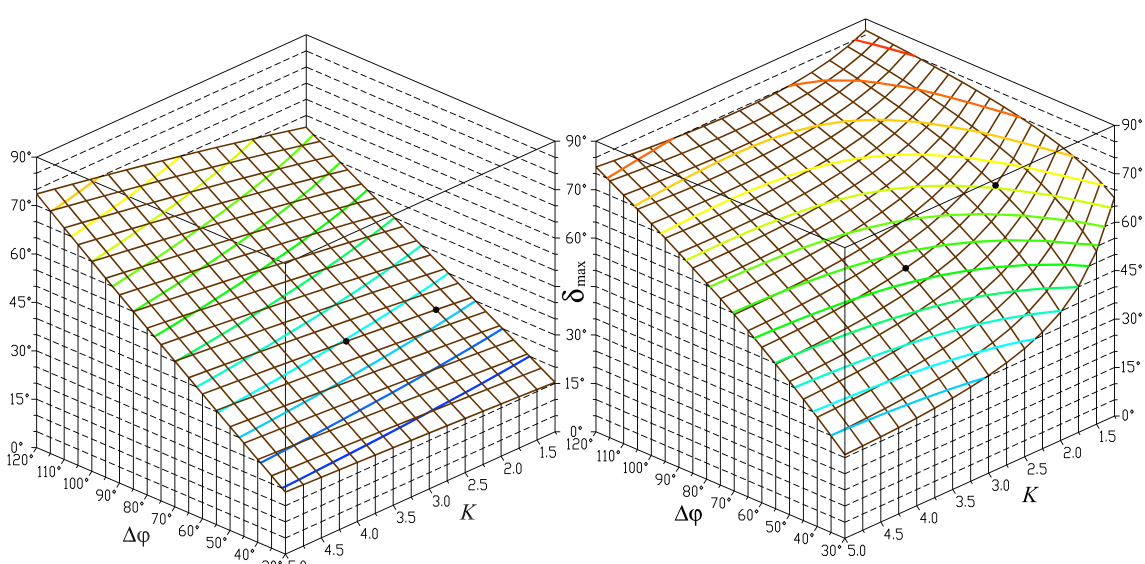

(**a**) (**b**)

Fig. 15. Maximum transmission angle deviation of the centric RPRR mechanisms optimized for uniform motion. Plot (**a**) corresponds to short rocker mechanisms and plot (**b**) corresponds to long rocker mechanisms.

to verify that the deviation from 90° of transmission angle μ is within acceptable limits.

(2) Draw three collinear points A, B_s and B_f (in this order) with AB_s equal to the minimum length of the linear actuator, and AB_f equal to the maximum length of the actuator.

(3) Locate point O along the perpendicular raised from the middle of segment B_sB_f such that the angle $\angle B_sOB_f$ equals to the desired rocker swing Δφ.

3.3. Design procedure of long-rocker RP̲RR mechanism with optimum transmission angle

Oscillating-slide mechanisms of the long-rocker type are recommended when compact arrangements are sought for, in association with actuators having large extension-coefficients. A quick synthesis method will be described for combination of Δφ and *K* that satisfy inequality (14), cases in which, according to Fig. A2, *OA* = *OB* = 1.

The Law of Cosine applied to the initial and final mechanism loop yields

$$\left(\frac{AB_f}{AB_s}\right)^2 = \frac{1-\cos(\varphi_s+\Delta\varphi)}{1-\cos\varphi_s} \tag{18}$$

which has been rearranged as

$$\frac{1-\cos(\varphi_s+\Delta\varphi)}{1-\cos\varphi_s} - K^2 = 0 \tag{19}$$

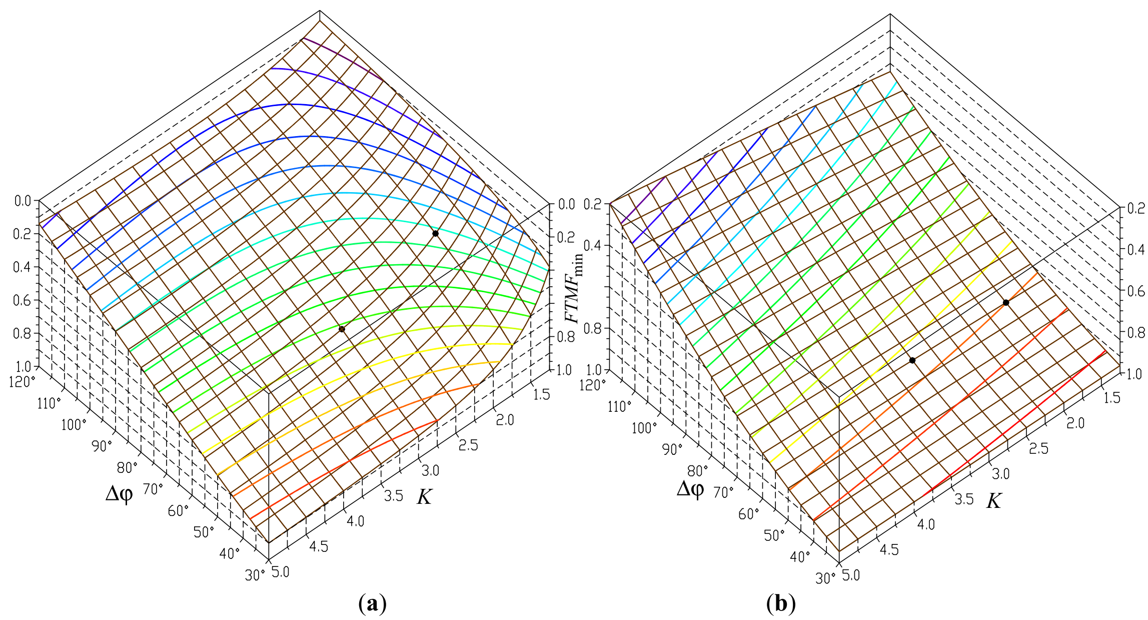

Fig. 16. TFMF of the centric RP̲RR mechanisms optimized for uniform motion. Plot (**a**) corresponds to short rocker mechanisms and plot (**b**) corresponds to long rocker mechanisms.

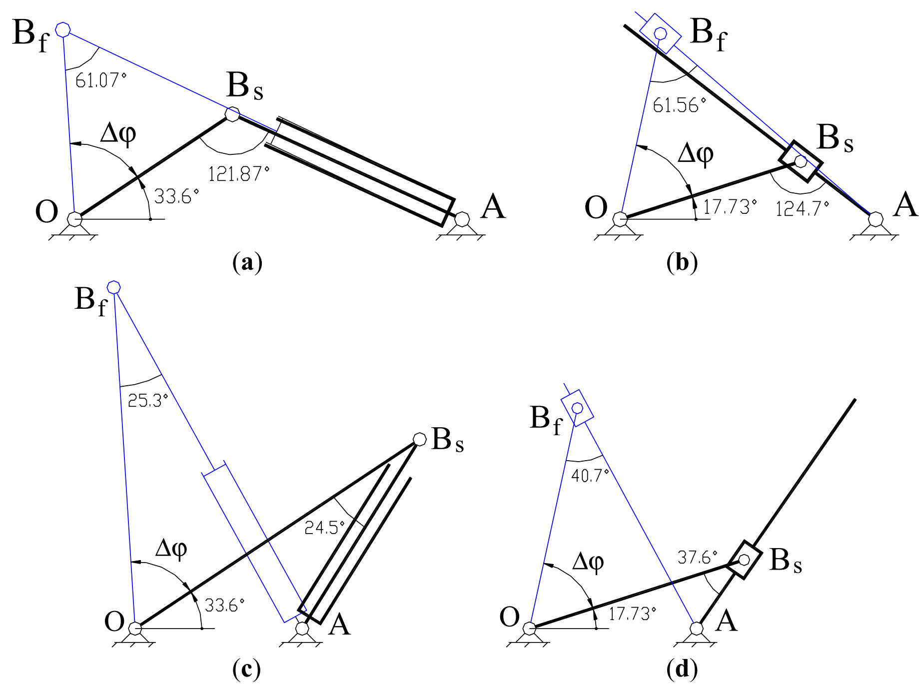

Fig. 17. Optimum mechanisms in Table 2, scaled such that their linear motor displacements ΔS_{max} are the same.

For a given extension coefficient K and angle of swing $\Delta\varphi$ of the rocker, Eq. (19) can be solved iteratively in the unknown φ_s.

Note that in the search for an optimum RP̲RR mechanism configuration, the extension coefficient K may be adjusted as well i.e. the designer can experiment with multiple linear actuators available from catalogs, or customize one actuator to match the desired extension-coefficient.

4. Centric RP̲RR mechanism actuators optimized for mechanical advantage

As mentioned earlier, when the rocker swing $\Delta\varphi$ is imposed a fix value in a RP̲RR mechanism, there is only one parameter (i.e. the initial angle φ_s of the rocker) that can be modified in the process of satisfying additional design requirements. In this section the case where a maximum *mechanical advantage* (also equal to the *force-to-torque multiplication factor*) must be attained will be considered. This corresponds to maximizing the function $FTMF_{min}$ with respect to φ_s. The number of displacement steps n of the actuator in Eq. (11) has been considered equal to five times the rocker swing in degrees (i.e. for $\Delta\varphi = 60°$, $n = 300$). Repeated maximizations of $FTMF_{min}(\varphi_s)$ have been performed and the resulting data served to generate the plots in Figs. 9–11 and in Appendix B.

Coincidently, the *ha-ha-wall* type discontinuities visible in Fig. 10a, 11a, A4a, A5a and A6a (the short-rocker RP̲RR mechanisms) occur for the same combinations of $\Delta\varphi$ and K in inequality (16). Also notice that the area inside the *ha ha* corresponds to $OA = AB = 1$ (Fig. A5a), a fortuitous combination which simplifies the design process.

The proportions of the RP̲RR mechanisms optimized for mechanical advantage can be extracted from the 3D plots in Appendix B, while their transmission angle and linearity error performances can be verified using the 3D plots in Figs. 9–11. Alternative to using the 3D design charts in Appendices A–C, the $FTMF_{min}$ function in Eq. (11) can be maximized anew for a given extension coefficient K and rocker angle $\Delta\varphi$. Easier in this regard is to tabulate $FTMF$ vs. φ_s in Eq. (10) and extract its maximum point.

As the 3D plots in Figs. 9–11 show, if an improved $FTMF$ is desired and the freedom exists, then extension coefficient K should be increased, and the rocker angle $\Delta\varphi$ should be reduced (less for the long rocker RP̲RR mechanisms the $FTMF$ of which does not depend on $\Delta\varphi$). The same changes in K and $\Delta\varphi$ will cause an improvement in δ_{max} and ε_{max}.

Sample mechanisms with $\Delta\varphi = 60°$, $K = 1.75$ and $K = 3.0$ that exhibit best mechanical advantage performances are shown in Figs. 12 and 13. Their geometric parameters are available in Table 2, and have also been marked with dots on the surface plots in Figs. 9–11 and A4–A6. Animated GIFs of Fig. 12 are available for download from the author's *ResearchGate* page.

5. Centric RP̲RR mechanism actuators optimized for uniform motion

The last design requirement of a RP̲RR mechanism discussed in this paper is where a near linear correlation between input and

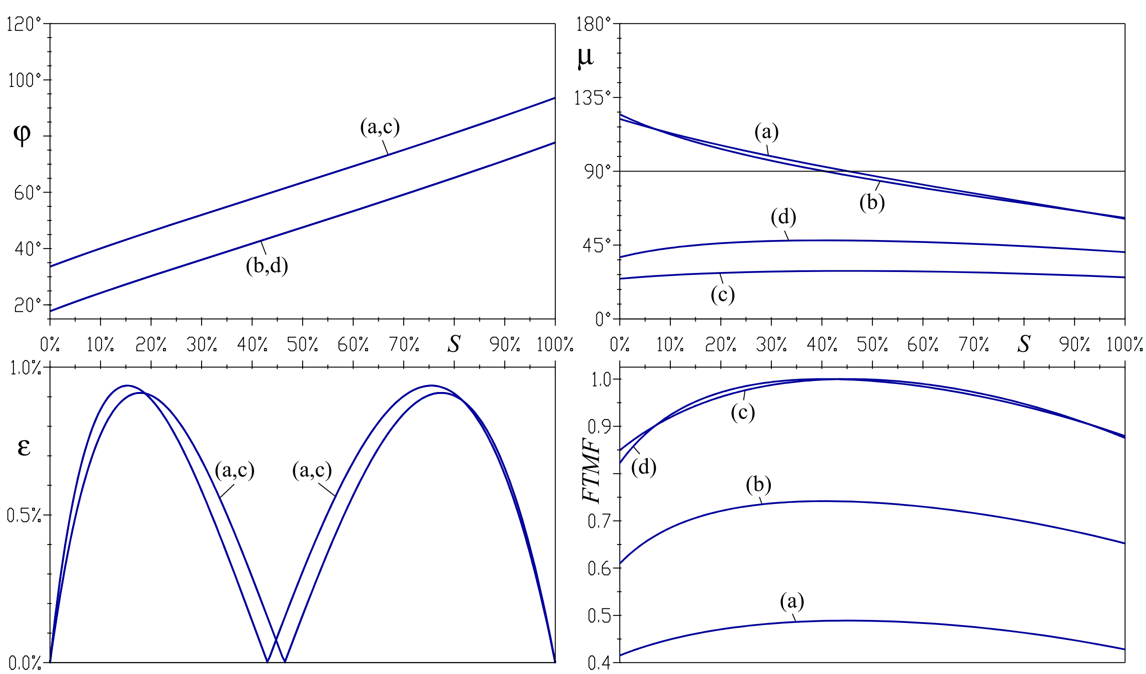

Fig. 18. Kinematic and performance diagrams of the mechanisms in Fig. 17, labeled the same as in Table 3 and in Fig. 17.

Table 3
Examples of RP̲RR mechanisms with $\Delta\varphi = 60°$, $K = 1.75$ and $K = 3$ optimized for linearity error.

		K	φ_s (°)	OA	OB	AB_s	δ_{max} (°)	ε_{max} (%)	$FTMF_{min}$
(a)	Short rocker	1.75	33.60	1.0	0.488867	0.651625	31.87	0.91	0.415
(b)	Short rocker	3.00	17.73	1.0	0.741640	0.370405	34.70	0.94	0.610
(c)	Long rocker	1.75	33.60	1.0	2.045545	1.332928	65.47	0.91	0.849
(d)	Long rocker	3.00	17.73	1.0	1.348363	0.499440	52.43	0.94	0.822

output link motions must be satisfied. For this, the maximum linearity error function $\varepsilon_{max}(\varphi_s)$ in Eq. (14) has been minimized using the same grid search followed by Brent's *Localmin* algorithm. The number of displacement steps of the liner actuator was again set equal to five times the angle $\Delta\varphi$ in degrees. Repeated minimizations of objective function $\varepsilon_{max}(\varphi_s)$ resulted in the 3 D plots in Figs. 14–16 and in Figs. A7–A9 in Appendix C. According to these, there is no obvious link-length correlation to simplify the synthesis process. The proportions of the optimized RPRR mechanisms can be however extracted from the 3D plots in Appendix C, while their expected performance can be checked using the diagrams in Figs. 14–16.

Long and short RPRR mechanisms exhibit identical linearity error performance (Fig. 14), which do not depend on *K* but can be improved by reducing rocker angle $\Delta\varphi$. A reduction of $\Delta\varphi$ also improves δ_{max} and overall *FTMF* for both short and long RPRR mechanisms Increasing *K* also improves δ_{max} and *FTMF*, less for short RPRR mechanisms where increasing *K* cause a slight increase in δ_{max}.

Rather than using the design charts in Appendix C, the linearity-error function $\varepsilon_{max}(\varphi_s)$ in Eq. (14) can be minimized anew for a given extension coefficient *K* and rocker angle $\Delta\varphi$. The expected maximum deviation from 90° of transmission angle μ and $FTMF_{min}$ can be extracted from the 3D plots in Figs. 15 and 16.

Sample mechanisms that exhibit minimum I/O linearity error are provided in Figs. 17 and 18. Their geometric parameters are summarized in Table 3, and are also marked with dots on the surface plots in Figs. 14–16 and in Appendix C. See also the *Research-Gate* page of the author where animated GIFs of Fig. 17 have been posted.

6. Conclusions

Detailed kinematic syntheses procedures of the centric oscillating-slide RPRR mechanism actuators for best transmission angle, maximum mechanical advantage and minimum I/O linearity error have been presented. Optimization problems have been formulated and solved numerically for these mechanisms. Two configurations have been shown to exist, one with a relatively short-rocker, and the other one with a longer rocker.

Parametric design charts and easily-applicable design procedures have been also provided in the paper. Also provided were bivariate performance charts, which allow a convenient overview upon the capabilities of these mechanisms, useful to guide the search when the angle of swing of the rocker, or the extension coefficient of the actuator do not have strictly imposed values.

Conflict of interest

The author declares no potential conflicts of interest with respect to the research, authorship, and/or publication of this article.

Appendix A

Geometric parameters of the oscillating-slide mechanisms optimized for transmission angle. Plots (**a**) correspond to the short-rocker- and plots (**b**) to the long-rocker-mechanism solutions (see Figs. A1–A3).

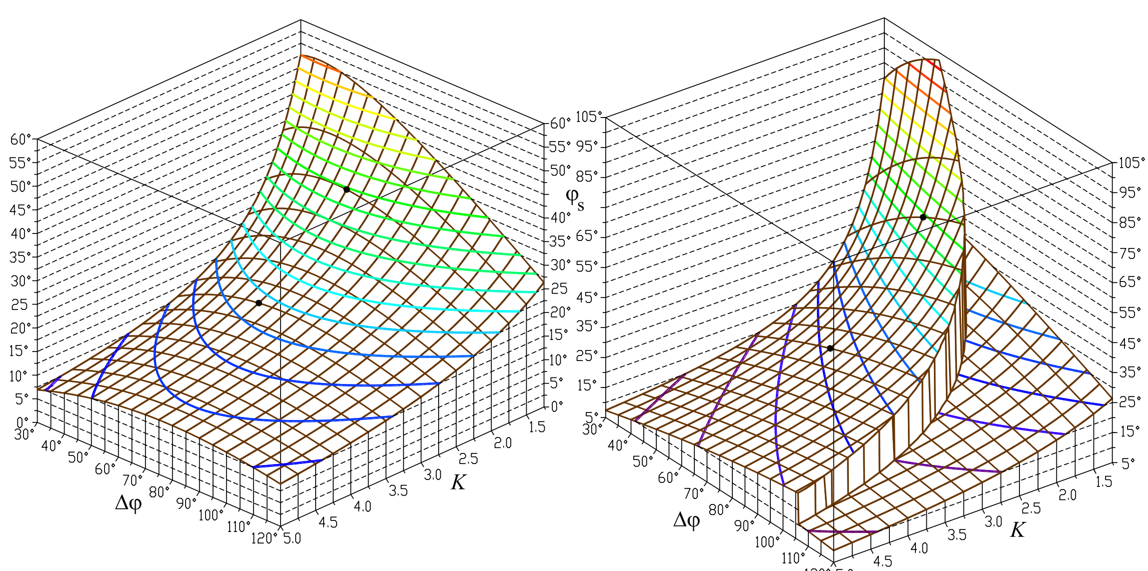

(**a**) (**b**)

Fig. A1. Initial rocker angle φ_s.

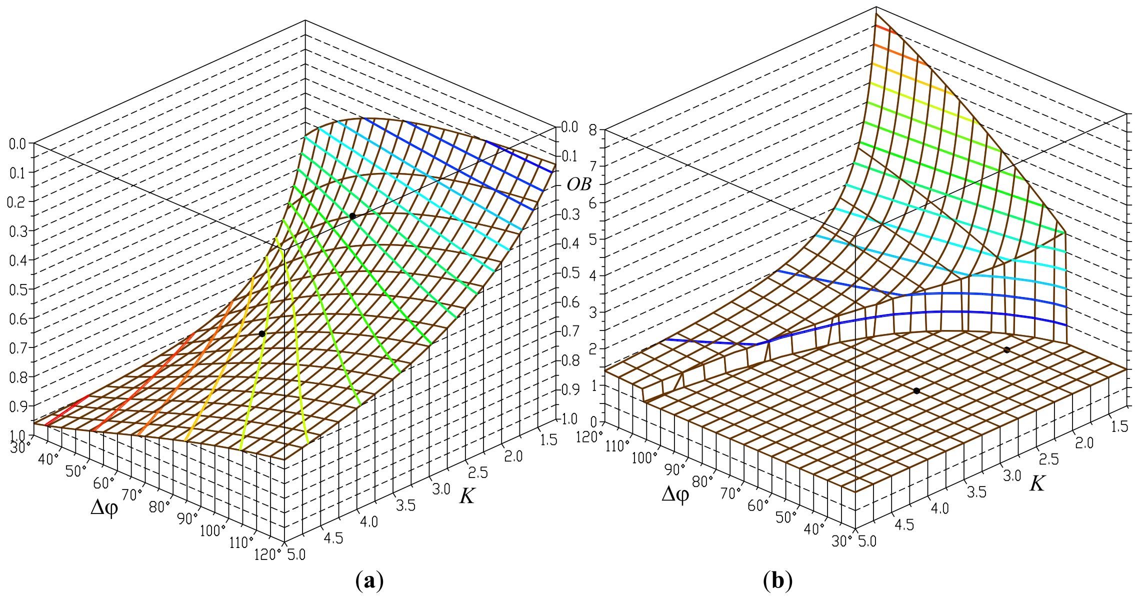

Fig. A2. Normalized rocker length OB.

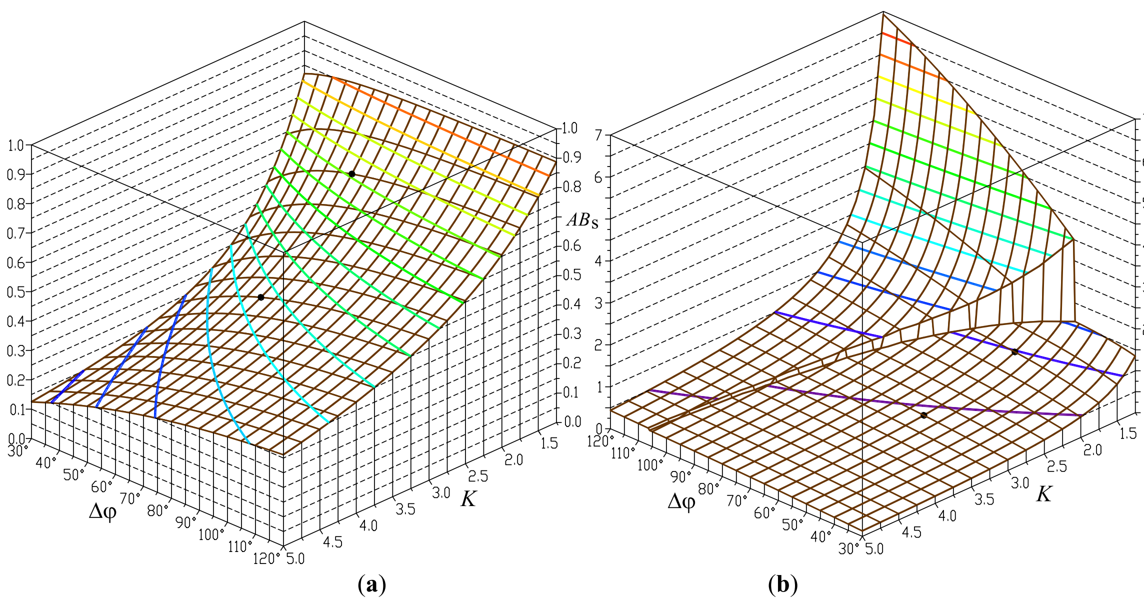

Fig. A3. Normalized length of the fully retracted actuator AB_s.

Appendix B

Geometric parameters of the oscillating-slide mechanisms optimized for *FTMF*. Plots (**a**) correspond to the short-rocker- and plots (**b**) to the long-rocker-mechanism solutions (see Figs. A4–A6).

Appendix C

Geometric parameters of the oscillating-slide mechanisms optimized for uniform motion. Plots (**a**) correspond to the short-rocker- and plots (**b**) to the long-rocker-mechanism solutions (see Figs. A7–A9).

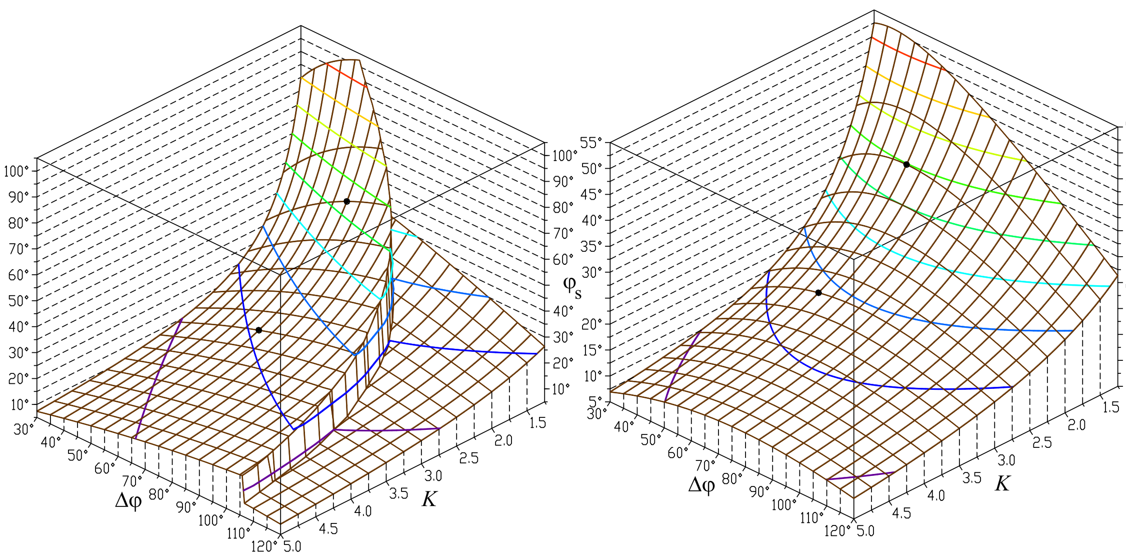

(**a**) (**b**)

Fig. A4. Initial rocker angles φ_s.

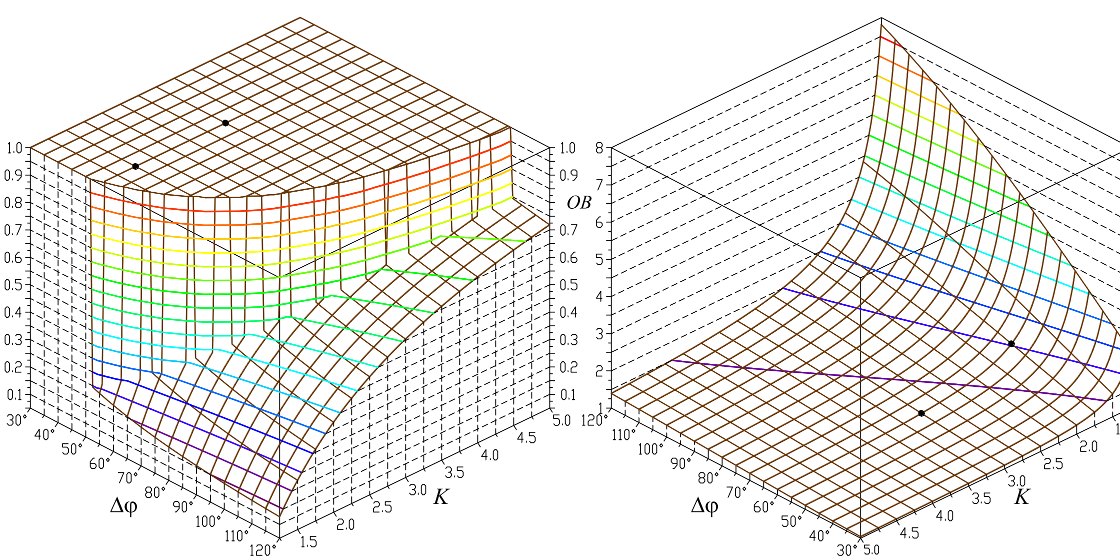

(**a**) (**b**)

Fig. A5. Normalized rocker length OB.

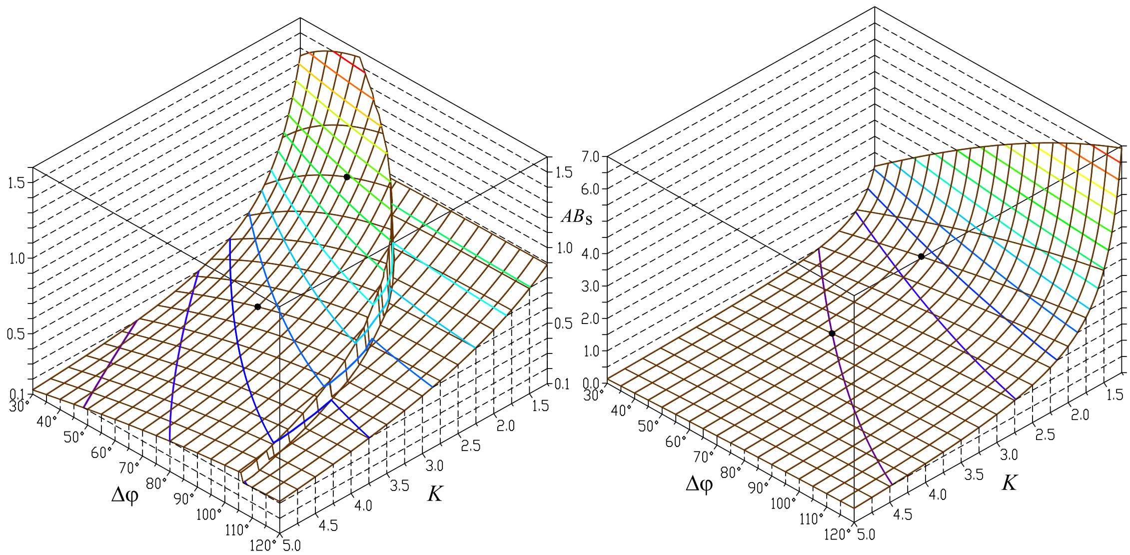

Fig. A6. Normalized length of the fully retracted actuator AB_s.

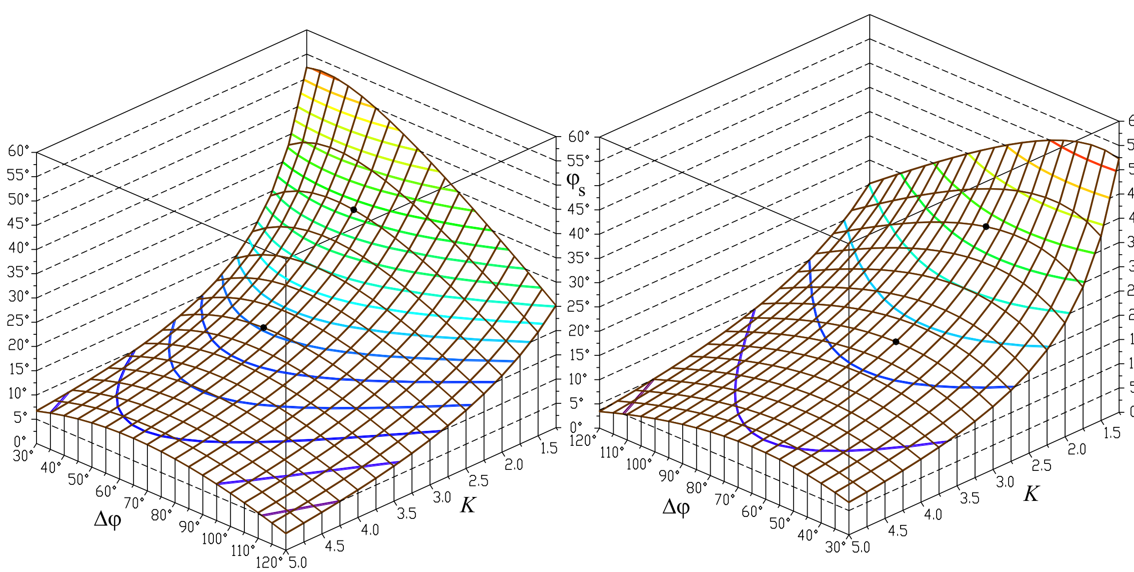

Fig. A7. Initial rocker angles φ_s.

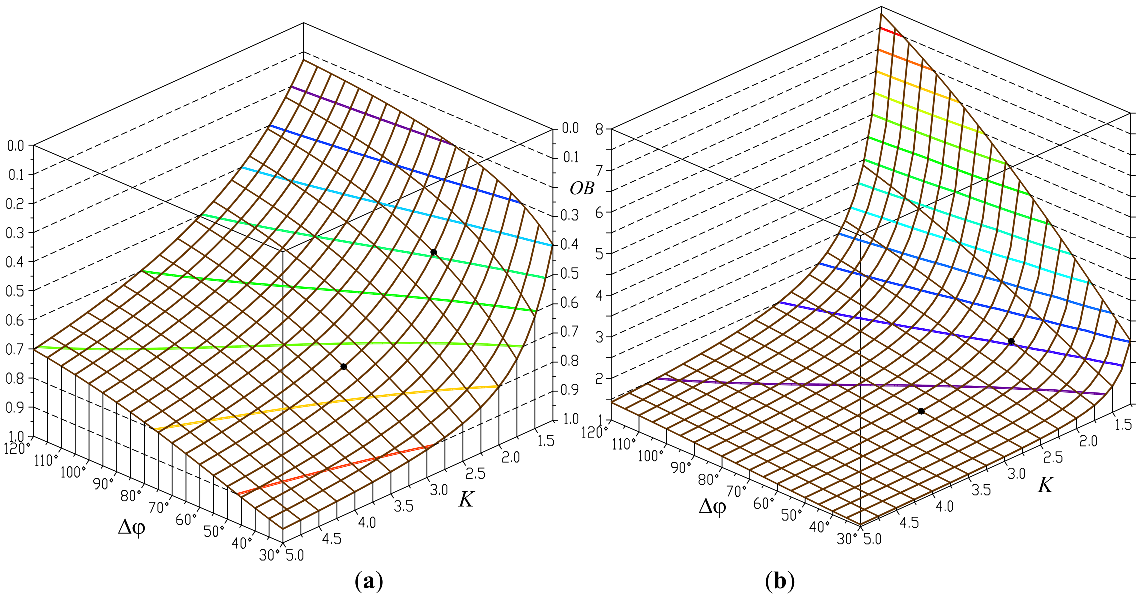

Fig. A8. Normalized rocker length OB.

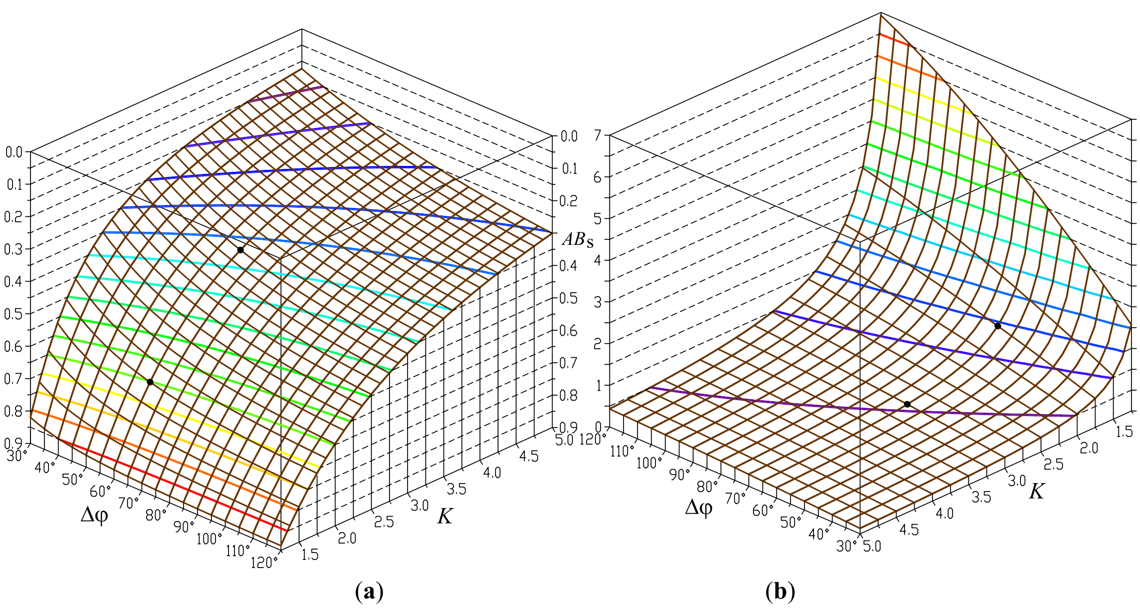

Fig. A9. Normalized length of the fully retracted actuator AB_s.

References

Bagci, C. (1987). Synthesis of linkages to generate specified histories of forces and torques-the planar slider-rocker mechanism. In *Proceedings of the 13th ASME DETC 10-2* (pp. 237–244).

Brent, R. P. (2013). *Algorithms for function minimization without derivatives*. Mineola, NY, USA: Dover Publications.

Eagle Hydraulic Components Inc. (2016). *Catalog*. Mirabel, QC, Canada.

Ergo-Help Pneumatic (2016). *Catalog*. Arlington Heights, IL, USA.

Hain, K. (1960). Die Bedeutung eines Getriebeatlasses über Vierwinkelfunctionen von Gelenkvierecken an Hand von Beispielen aus dem Landmaschinenbau. *Grundlagen der Landtechnik Heft, 12*, 37–45.

Hain, K. (1968). Zur Weiterentwicklung der Ladegeräte mit hydraulischen Schubkolbenantrieben. *Landbauforschung Völkenrode, 18*, 79–82.

Hartenberg, R. S., & Denavit, J. (1964). *Kinematic synthesis of linkages*. New York, USA: McGraw-Hill.

Karlsson, A., & Gilmer, T. (2017). Using embedded CAN bus to control electro-mechanical actuators in off-highway applications. *Product Design & Development (www.pddnet.com)*. Feb. 2017, www.pddnet.com/news/2017/02/using-embedded-can-bus-control-electromechanical-actuators-highway-applications.

Parker Hannifin Corp (2009). *Mobile Cylinder Div. Catalog HY18-0014*, Youngstown, OH, USA.

Reifschneider, L. G. (2005). Teaching kinematic synthesis of linkages without complex mathematics. *Journal of Industrial Technology, 21*(4), 1–16.

Sandor, G. N., & Erdman, A. G. (1984). *Advanced mechanism design: Analysis and synthesis*. Upper Saddle River, NJ, USA: Prentice Hall.

Simionescu, P. A. (1999). *Contributions to the optimum synthesis of linkage-mechanisms with applications* Doctoral Dissertation. University Politechnica of Bucharest.

Simionescu, P. A. (2014). *Computer-aided graphing and simulation tools for AutoCAD users*. Boca Raton, FL, USA: Chapman & Hall/CRC.

Simionescu, P. A. (2016). Design of planar slider-rocker mechanisms for imposed limit positions, with transmission angle and uniform motion controls. *Mechanism and Machine Theory, 97*, 85–99.

Simionescu, P. A., & Smith, M. R. (2000). Single-valued function representations in linkage mechanisms design. *Mechanism and Machine Theory, 35*(12), 1709–1726.

SKF (2016). *Linear motion catalog*. Sweden: Gothenburg.
Söylemez, E. (2009). *Mechanisms*. Ankara, Turkey: Middle East Technical University, METU Publication #64.
Söylemez, E., & Tönük, E. (1993). Design of piston driven six-link mechanisms with large swing angle and optimum transmission. *Proceedings of the 6th international symposium theory and practice of mechanisms, Bucharest, June 1–5* (Vol. 1, pp. 301–308). .
Tao, D. C. (1964). *Applied linkage synthesis*. Boston, MA, USA: Addison-Wesley.
Texas Hydraulics (2016). *Catalog*. Temple, TX, USA.
Ultra Motion (2016). *Catalog*. Cutchogue, NY, USA.
Volmer, J. (1978). *Getriebetechnik leitfaden*. Braunschweig, Germany: Vieweg & Teubner Verlag.
Yu, W.-J., Huang, C.-F., & Chieng, W.-H. (2004). Design of the swinging-block and turning-block mechanism with special reference to the mechanical advantage. *JSME International Journal, Series C, 47*(1), 363–368.
Zhang, Z., & Zhang, Y. (2012). Repetitive motion planning and control on redundant robot manipulators with push-rod-type joints. *ASME, Journal of Dynamic Systems, Measurement, and Control, 135*(2), 024502. Nov 07.